This paper describes objective technical results and analysis. Any subjective views or opinions that might be expressed in the paper do not necessarily represent the views of the U.S. Department of Energy or the United States Government.

SAND2019-6847C

Maximum pit size prediction for environments relevant to stainless steel casks: determination of pit stability and repassivation potential

Ryan M. Katona
Center for Electrochemical Science and Engineering || University of Virginia
Storage and Transportation Technology || Sandia National Laboratories

Objectives

- Determine maximum pit size as a function of chloride concentration and temperature
- Determine cathodic kinetics as a function of chloride concentration and temperature
- Combine both anodic and cathodic kinetics to determine the maximum pit size of in environments seen on stainless steel 304/304L in marine environments

Motivation

- Stainless Steels (SS) of various grades are used in a wide range of applications and are seen in environmental conditions.
  - Stainless steels are subject to localized pitting corrosion
- Recent interest has been focused on the storage of spent nuclear materials
  - Stainless steel grades 304, 316, and their low carbon counter parts are used and are currently in storage (Figure 1)

Figure 1: Stainless Steel Cask

- Casks are reaching the end of their commissioned lifetimes and currently assessment and prediction of future lifetimes of the canisters is underway
  - Due to spatial constraints, it is not always possible to reach all parts of the canister to asses damage.
- Prediction of localized corrosion is key to understanding overall life times and performance
- Understanding both chloride and temperature dependencies of maximum pit size can help predict the current state of pitting corrosion and associated stress intensities for pit to crack transitions

Previous Work

- A maximum pit size model has been set forth by Chen and Kelly exploiting the inherent coupling of an anode to its surrounding cathode [ref]
- Woldemidhen et al. explored maximum pit size as a function of FeCl3 concentration at room temperature [ref]
- (ix)_sf and DC have been explored as a function of temperature in 1M NaCl [ref]
- FeCl2 solubility have been explored as a function of temperature
- A wide range of temperatures and chloride concentration has not been taken into account in previous studies

Anodic Kinetics Determined by Lead in Pencil Techniques

Galvele Pit Stability Product Determination

- Based on 1-dimensional diffusion of a simulated pit, the limiting current density is related to the diffusion of metal ions (D_{M^+}), concentration gradient of metal ions ($C_{sat}^{M^+}$), the number of electrons transferred (n), pit depth (d) and Fradays constant

$$i_{lim} = \frac{nFD_{M^+}C_{sat}^{M^+}}{d} = (i \cdot x)_{sf}$$

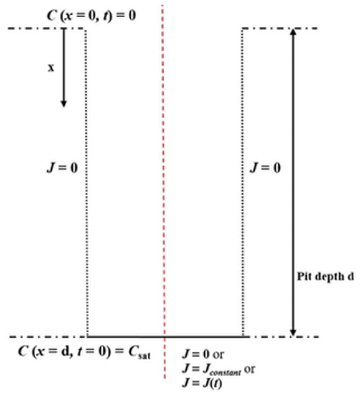

Figure 2: Galvele Pit Stability – Assumptions made in determine pit stability product

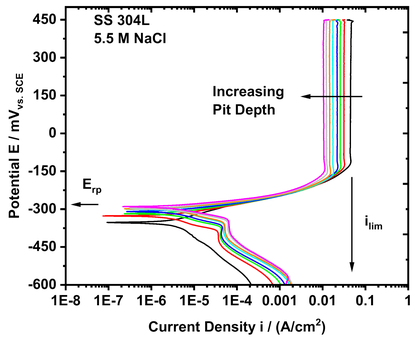

Figure 3: Cathodic Scans following pit growth – Fast cathodic scan (5 mV/sec) after anodic pit growth

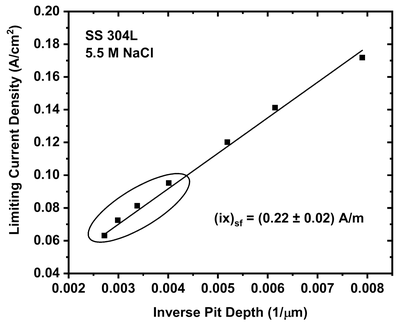

Figure 4: Determination of pit stability product– Limiting current density vs. (1/d) to determine $(i \cdot x)_{sf}$

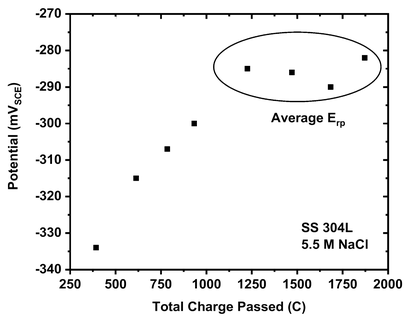

Figure 5: Determination of Repassivation potential– Plateau of E_{rp} with sufficient current passed

- SS304L wires (diameter = 50 μm) were mounted in epoxy, initiated growth by anodic holds at 750 mV_{SCE}, propagated at 450 mV_{SCE}, and a cathodic scan at 5 mv/sec was conducted to gain parameters of interest
- Pit stability ($(i \cdot x)_{sf}$) was determined for NaCl and $MgCl_2$ solutions spanning a range of 25°C to 55°C

Cathodic Kinetics and Maximum Pit Size Calculations

Cathodic Kinetics

- Cathodic kinetics were determined in NaBr solutions containing the same quantity of $D_{O_2}^{2/3} C_{O_2} \nu^{-1/6}$ as NaCl solutions in order to match i_{lim}

Maximum Pit Calculations

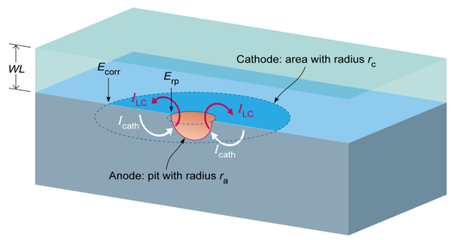

Figure 6: Schematic of maximum pit model– Coupled anode and cathode under finite water layer

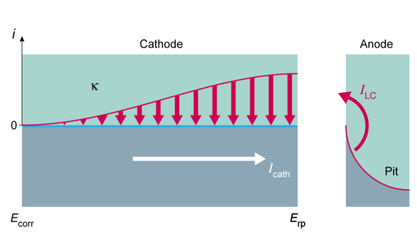

Figure 7: Current Distribution – Current supply for an anode from finite cathode

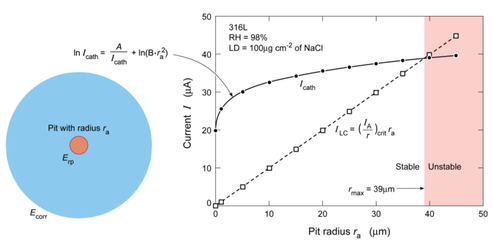

Figure 8: Cathode and Anode Kinetics– Stable max pit given by I_cath and (ix) intersection

Max. Cathode Current · Brine Conductivity · Brine Thickness · Cathodic Kinetics

$$\ln(I_{c,max}) = \frac{4\pi k(\mathrm{WL})\Delta E_{max}}{I_{c,max}} \cdots + \ln\left[\frac{\pi e r_a^2 \int_{E_{corr}}^{E_{rp}} (i_c - i_p)dE}{\Delta E_{max}}\right]$$

Cathodic Area

$$\ln(S_{ceq,min}) = \frac{\left(\frac{4\pi k(\mathrm{WL})(\Delta E_{max})^2}{\int_{E_{corr}}^{E_{rp}} (i_c - i_p)dE}\right)}{S_{ceq,min}} \cdots + (1 + \ln\pi + 2\ln r_a)$$

Cathodic Radius

$$R_{c,min} = \sqrt{\frac{S_{ceq,min}}{\pi}}$$

- In order to determine maximum pit size of a given alloy in desired solutions, the conductivity, cathodic kinetics, relative humidity, pit stability product, and repassivation potential need to be determined.
- OLI Studio was used in order to determine conductivity and conductivity while anodic cathodic kinetics were determined by lead in pencil experiments and NaBr scans respectively.

(ix)Sf and DC decrease with increasing [Cl-] and increase with increasing temperature

Pit stability product and DC

- Determination of $(i \cdot x)_{sf}$ and $D_{M^+}C_{sat}^{M^+}$ as a function of [Cl^-] and temp.[(a)] It is noted that $(i \cdot x)_{sf}$ and $D_{M^+}C_{sat}^{M^+}$ are equivalent expressions.

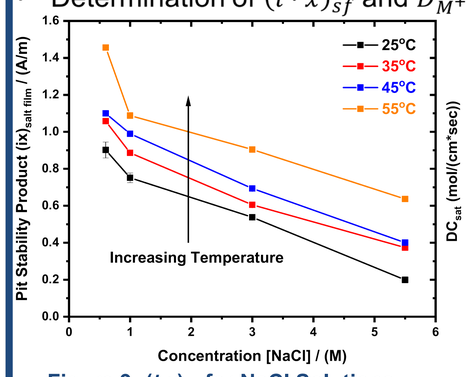

Figure 9: $(i \cdot x)_{sf}$ for NaCl Solutions

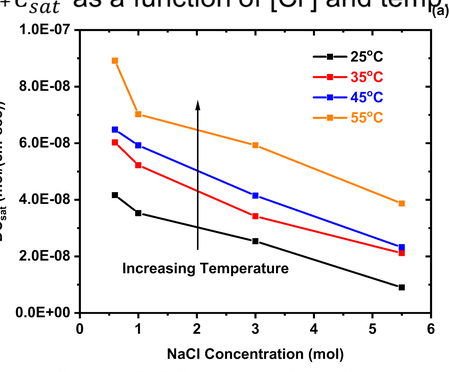

Figure 10: DC for NaCl Solutions

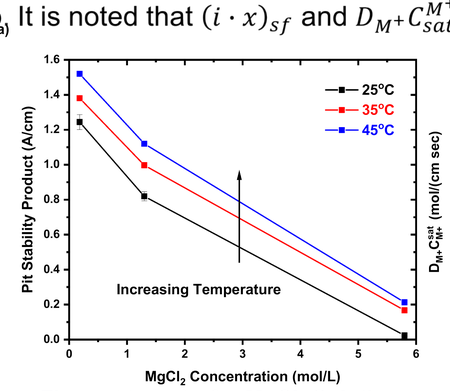

Figure 11: $(i \cdot x)_{sf}$ for $MgCl_2$ Solutions

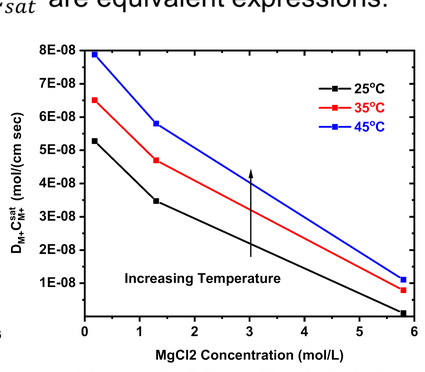

Figure 12: DC for $MgCl_2$ Solutions

Sandia National Laboratories is a multi-mission laboratory managed and operated by National Technology and Engineering Solutions of Sandia, LLC., a wholly owned subsidiary of Honeywell International, Inc., for the U.S. Department of Energy's National Nuclear Security Administration under contract DE-NA0003525.

Sandia National Laboratories is a multimission laboratory managed and operated by National Technology & Engineering Solutions of Sandia, LLC, a wholly owned subsidiary of Honeywell International Inc., for the U.S. Department of Energy's National Nuclear Security Administration under contract DE-NA0003525.

E_rp Decrease with Increasing [Cl-]

Repassivation Potential

- Decrease in E_{rp} with increasing [Cl-]

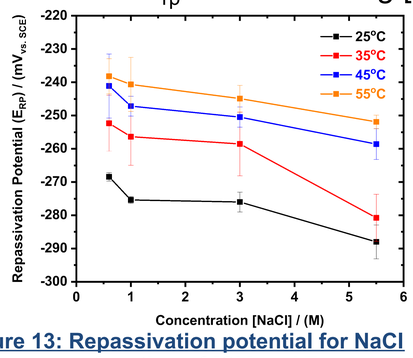

Figure 13: Repassivation potential for NaCl as a function of [Cl-] and T

Increase in E_{rp} with increasing [Cl-]

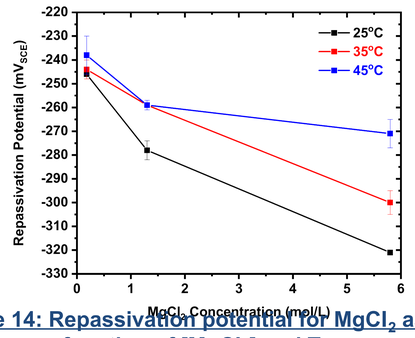

Figure 14: Repassivation potential for $MgCl_2$ as a function of [$MgCl_2$] and T

Determination of Cathodic Kinetics

Repassivation Potential

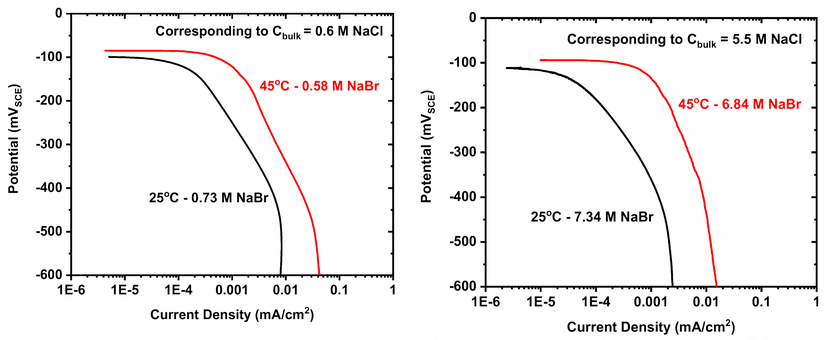

Figure 15: Cathodic Kinetics corresponding to (a) 0.6 M NaCl and (b) 5.5 M NaCl

Cathodic kinetics characterized by an increase in i_{lim} with increasing temperature

A decrease in is seen i_{lim} with increasing [NaBr]

- Increase in RH => increase cathode radius
- Decrease in [NaCl]decrease in conductivity => decrease in cathode radius
- A decreasing equivalent cathodic density => increase in cathode radius.
- Increase in chloride concentration => increase in pit size => increase in cathode radius

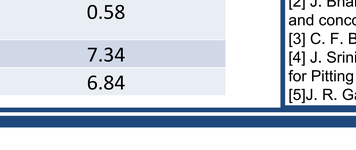

Figure 16: Environmental impacts on the cathode size: Impact of temperature and chloride concentration

Increase in Solubility with Increased Temperature

Determination of Saturation Concentration

- $FeCl_2$, $CrCl_3$, and $NiCl_2$ solubility in stoichiometric proportion to SS304L

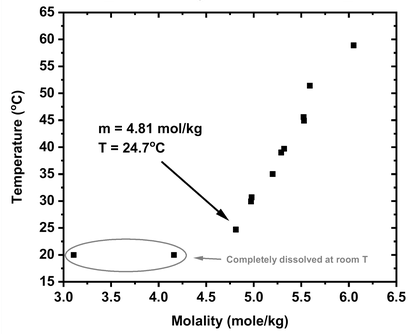

Figure 17: Solubility curve: Total molality represents stoichiometric concentrations of Fe^{2+}, Cr^{3+}, and Ni^{2+}

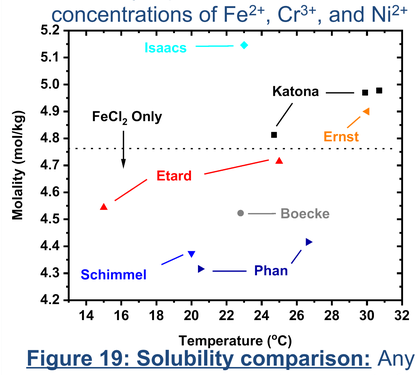

Figure 19: Solubility comparison: Any conversions were made with a density for saturated $FeCl_2$ of 1.44 g/cm³

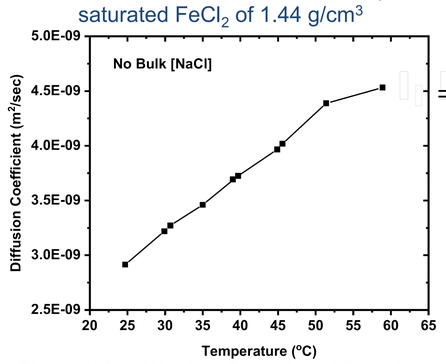

Figure 21: Diffusion Based on Einstein-Stokes: predicted D_{M+} based on solution viscosity

Increase in $C_{sat}^{M^+}$ with increased temperature.

At T = 24.7 °C, solubility of 4.81 mole/kg is achieved

Concentration of individual ions shown in Figure 18

Similar trend to $FeCl_2$ solutions however slightly increased molality as seen in Fig. 19.

Hydrolysis of metal cations accounts of decrease in pH with increasing solution molality

$$M^+ + H_2O \rightarrow M(OH) + H^+$$

Below pH of $FeCl_2$ solutions

Stokes-Einstein equation for diffusivity:

$$D_{M^+} = \frac{kT}{6\pi\eta_D r}$$

= dynamic viscosity

Saturation concentration as a function of bulk chloride

$$K_{sp} = [Me^{z+}][Cl^-]^z$$

Common ion effect decreases overall saturation concentration

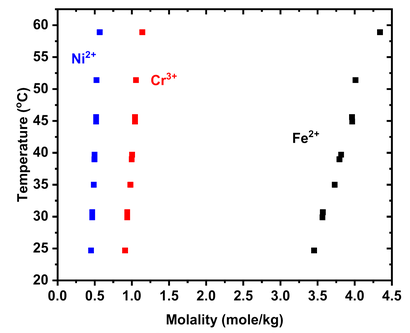

Figure 18: Solubility of individual ions: Molality of individual ions at saturation

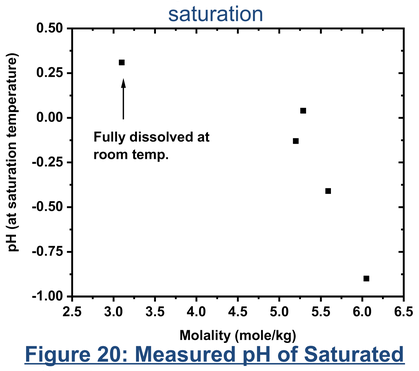

Figure 20: Measured pH of Saturated Solutions: pH measurements taken within 2 min of saturation (within 5°C)

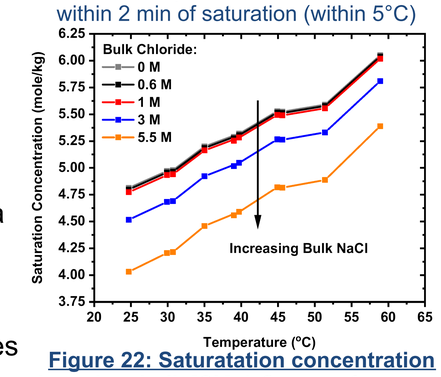

Figure 22: Saturatation concentration based on bulk [Cl-]: influence of common ion effect on saturation

Maximum Pit Determined for SS 304L

Maximum pit results

- Maximum pit parameters were determined for SS304L in varying NaCl solutions at multiple temperatures

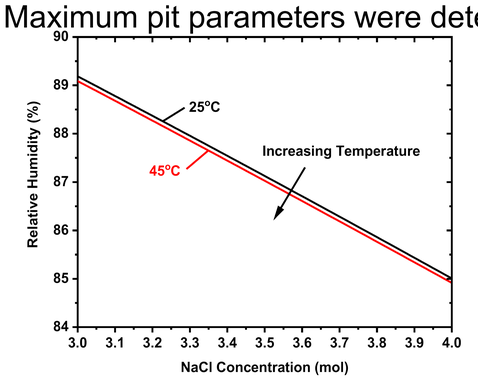

Figure 23: Calculated Relative Humidity

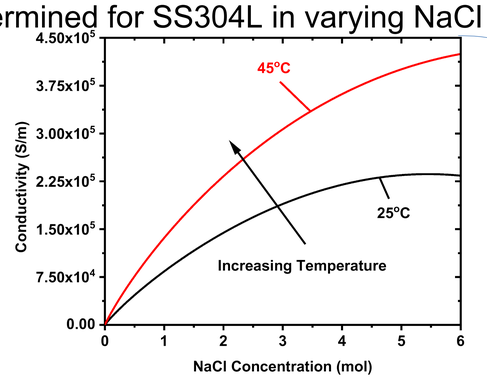

Figure 24: Calculated Conductivity

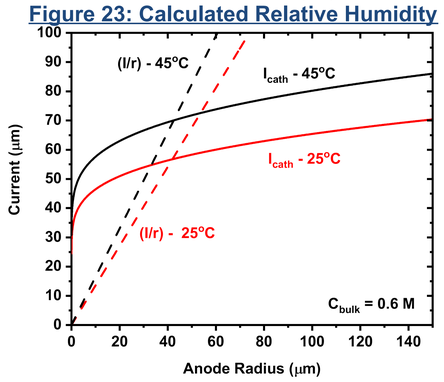

Figure 25: I_{cath} and I_{LC} for 0.6 M NaCl

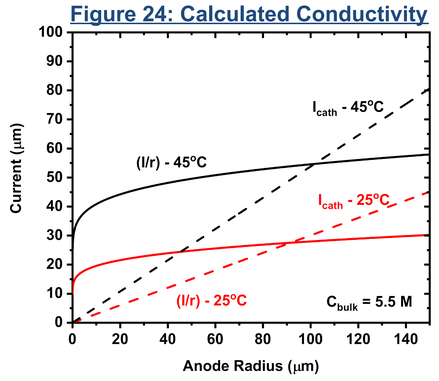

Figure 26: I_{cath} and I_{LC} for 5.5 M NaCl

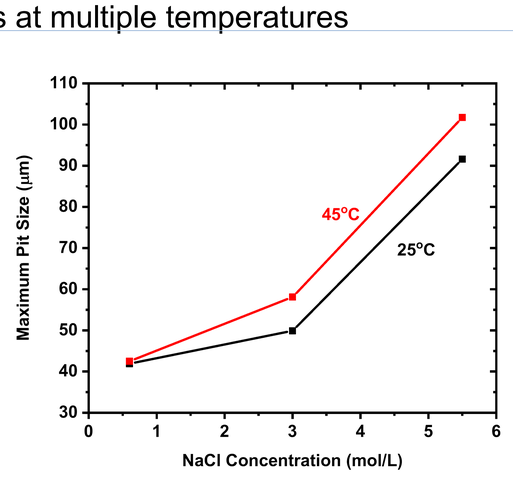

Figure 27: Calculated Maximum Pit Size

- Max pit size increase with [NaCl] and temperature
- Difference due to temperature at 5.5 M NaCl was much larger than 0.6 M.
- Only considering $(i \cdot x)_{sf}$ one would think that at elevated temperatures the pit size would be smaller.
- However, when considering the inherent galvanic coupling with a surrounding cathode, the pit sizes increase with temperature

Solution	Conductivity (S/m)	Relative Humidity (%)	NaBr Concentration (M)
0.6 M (25°C)	5.45	98.04	0.73
0.6 M (45°C)	8.91	98.03	0.58
5.5 (25°C)	23.63	78.41	7.34
5.5 (45°C)	41.44	78.39	6.84

Conclusions

- $(i \cdot x)_{sf}$ increased with temperature and decreased with [NaCl] and E_{rp} increased with temperature and decrease with [NaCl]
- Saturation concentration determined for $FeCl_2$ $CrCl_3$ and $NiCl_2$ and increased with increasing temperature
- Maximum pit sizes were shown to increase in elevated temperature and chloride environments in thin water layers

Future Work

- Extend framework to $MgCl_2$ as well as more complex salts like sea water
- Validation of this framework in highly controlled testing envrionments

Acknowledgements

- I would like to thank my advisor Dr. Robert G. Kelly (UVA) and Dr. Eric Schindelholz (SNL) for their guidance and support in this work. I would also like to thank Jacob Carpenter for his help in experimental work.
- Financial assistance Nuclear Regulatory Commission fellowship under grant number NRC-HQ-84-16-G-0037 is gratefully acknowledged

References

[1] E. McCafferty, Introduction to Corrosion Science. 2010.
[2] J. Bhandari et al., "Accelerated pitting corrosion test of 304 stainless steel using ASTM G48; Experimental investigation and concomitant challenges," J. Loss Prev. Process Ind., vol. 47, pp. 10–21, 2017.
[3] C. F. Baes and R. E. Mesmer, The Hydrolysis of Cations. New York: John Wiley & Sons Inc., 1976.
[4] J. Srinivasan, M. J. McGrath, and R. G. Kelly, "A High-Throughput Artificial Pit Technique to Measure Kinetic Parameters for Pitting Stability," J. Electrochem. Soc., vol. 162, no. 14, pp. C725–C731, 2015.
[5]J. R. Galvele, "Transport Processes and the Mechanism of Pitting of Metals," J. Echem. Soc., vol. 123, no. 4, p. 464, 1976.
[6] M. T. Woldemedhin, M. E. Shedd, and R. G. Kelly, "Evaluation of the Maximum Pit Size Model on Stainless Steels under Thin Film Electrolyte Conditions," J. Electrochem. Soc., vol. 161, no. 8, pp. 3216–3224, 2014.
[7] Z. Y. Chen and R. G. Kelly, "Computational Modeling of Bounding Conditions for Pit Size on Stainless Steel in Atmospheric Environments," J. Electrochem. Soc., vol. 157, no. 2, p. C69, 2010.